HHS Public Access

Author manuscript

Nat Med. Author manuscript; available in PMC 2018 August 12.

Published in final edited form as:

Nat Med. 2018 March ; 24(3): 304–312. doi:10.1038/nm.4479.

Transcriptional regulation of macrophage cholesterol efflux and atherogenesis by a long noncoding RNA

Tamer Sallam[1,2,*], **Marius Jones**[1], **Brandon J Thomas**[3], **Xiaohui Wu**[2], **Thomas Gilliland**[1], **Kevin Qian**[1], **Ascia Eskin**[4], **David Casero**[1], **Zhengyi Zhang**[1], **Jaspreet Sandhu**[1], **David Salisbury**[1,2], **Prashant Rajbhandari**[1], **Mete Civelek**[5], **Cynthia Hong**[1], **Ayaka Ito**[1], **Xin Liu**[3], **Bence Daniel**[6], **Aldons J Lusis**[2,4], **Julian Whitelegge**[7], **Laszlo Nagy**[6], **Antonio Castrillo**[8], **Stephen Smale**[3], and **Peter Tontonoz**[1,*]

[1]Department of Pathology and Laboratory Medicine, Molecular Biology Institute, University of California, Los Angeles, CA 90095

[2]Department of Medicine, Division of Cardiology, University of California, Los Angeles, CA 90095

[3]Department of Microbiology, Immunology, and Molecular Genetics, and Molecular Biology Institute, University of California, Los Angeles, Los Angeles, CA 90095

[4]Departement of Human Genetics, University of California, Los Angeles, CA 90095

[5]Center for Public Health Genomics, University of Virginia, Charlottesville, VA 22908, USA; Department of Biomedical Engineering, University of Virginia, Charlottesville, VA 22908, USA

[6]Sanford-Burnham-Prebys Medical Discovery Institute at Lake Nona; Department of Biochemistry and Molecular Biology, Research Center for Molecular Medicine, Orlando, FL

[7]Pasarow Mass Spectrometry Laboratory, NPI-Semel Institute, University of California, Los Angeles, California 90095

[8]Instituto de Investigaciones Biomédicas Alberto Sols, CSIC-Universidad Autónoma de Madrid, Unidad de Biomedicina-Universidad de Las Palmas de Gran Canaria (Unidad asociada al CSIC) and Instituto Universitario de Investigaciones Biomédicas y Sanitarias (IUIBS) de la ULPGC, Las Palmas de Gran Canaria, Spain

*Address for Correspondence: tsallam@mednet.ucla.edu, ptontonoz@mednet.ucla.edu.

Data Availability and Accession Code Availability Statement:
The source data used in the manuscript can be accessed using the following accession numbers: GSE98910 (RNA-seq) , GSE97207 (ATAC-seq), GSE104027(ChIP-Seq), microarray (GSE107977).

Author Contributions:
T.S. and P.T. conceived and designed the study, guided the interpretation of the results and the preparation of the manuscript. P.T. supervised the study and T.S. managed the daily experiments. X.W. performed most mouse experiments and data analysis including atherosclerosis study. T.S, M.J., T.G., K.Q., Z.Z., J.S., D.S., P.R., J.S., C.H., A.I., X.L. participated in various *in vivo* and *in vitro* macrophage experiments and data analysis. Bioinformatic data analysis performed by D.C. and A.E. B.T., X.L. and S.S. assisted with ChIP & ATAC-seq experiments including data analysis. J.W. performed the mass spectrometry analysis. B.D. and L.N. assisted with ChIP and performed experiments defining enhancer landscape at Abca1. A.C. performed ChIP-seq for LXR. M.C. and A.L. provided GWAS data and technical guidance with atherosclerosis analysis.T.S. and P.T. edited the manuscript with input from all authors. All authors discussed the results and approved the final version of the manuscript.

Competing Financial Interest Statement:
The authors declare no competing financial interest.

Abstract

Nuclear receptors regulate gene expression in response to environmental cues, but the molecular events governing the cell-type specificity of nuclear receptors remain poorly understood. Here we outline a role for a non-coding RNA in modulating the cell type-specific actions of LXRs, sterol-activated nuclear receptors that regulate the expression of genes involved in cholesterol homeostasis and that have been causally linked to the pathogenesis of atherosclerosis. We identify the lncRNA MeXis as an amplifier of LXR-dependent transcription of the critical cholesterol efflux gene *Abca1*. Mice lacking the *MeXis* gene show reduced *Abca1* expression in a tissue-selective manner. Furthermore, loss of MeXis in mouse bone marrow cells alters chromosome architecture at the *Abca1* locus, impairs cellular responses to cholesterol overload, and accelerates the development of atherosclerosis. Mechanistic studies reveal that MeXis interacts with and guides promoter binding of the transcriptional coactivator DDX17. The identification of MeXis as a lncRNA modulator of LXR-dependent gene expression expands our understanding of the mechanisms underlying cell-type selective actions of nuclear receptors in physiology and disease.

Introduction

The accumulation of excess cholesterol by macrophages within the arterial wall is a pivotal step in the pathogenesis of atherosclerosis. The ability of macrophages to integrate metabolic and immune signaling in response to environmental cues and lipid excess is therefore an important determinant of disease susceptibility[1-23]. LXRs are ligand-dependent transcription factors that regulate expression of genes involved in macrophage responses to cholesterol, and also modulate inflammatory signaling [4,5]. Activation of LXRs promotes reverse cholesterol transport through induction of a cadre of genes, including *Abca1*, which encodes the plasma membrane transporter ABCA1. This ATP-dependent transporter is critical for HDL generation and its function is compromised in Tangier disease, a syndrome characterized by both HDL deficiency and accelerated atherosclerosis [6,7].

LncRNAs have been shown to function through diverse mechanisms, including exerting direct transcriptional effects in response to environmental cues [8]. A number of lncRNAs have been shown to regulate the expression of neighboring genes; however, the mechanisms by which noncoding gene activation serve local regulatory functions remain to be fully clarified [9,10]. Although a number of lncRNAs have been shown to have sequence-specific features, recent work highlights the strong contribution of neighboring promoter activity, including the processes of transcriptional initiation and splicing, on gene expression [11]. In this work we characterize an LXR-responsive lncRNA that affects transcriptional pathways linked to macrophage cholesterol efflux and atherosclerosis. Our results suggest that cell-type selective action of lncRNAs may contribute to the temporal and spatial gene activation patterns of nuclear receptors.

Results

Regulation of macrophage lncRNAs in response to cholesterol loading

LXRs influence the expression of a large repertoire of genes linked to lipid metabolism in a context-specific fashion. We noted that the gene encoding critical cholesterol efflux mediator

ABCA1 was much more highly induced by synthetic LXR in macrophages than in other cell types such as hepatocytes and adipocytes (Supplementary Fig. 1a). To gain insight into the basis for this cell-type selective LXR response, we performed genome-wide transcriptional profiling on mouse peritoneal macrophages treated with or without the synthetic LXR agonist GW3965. The expression of canonical protein-coding LXR target genes was robustly induced by LXR agonist treatment, as expected (Supplementary Fig. 1b). Consistent with established roles of LXR in metabolism, the network of ontology terms for GW3965-induced genes showed robust enrichment for lipid regulatory processes and macrophage-specific pathways (Supplementary Fig. 1c). Interestingly, we also observed that LXR activation induced a limited number of lncRNAs (Supplementary Fig. 1d and Supplementary Table 1). Several of these lncRNAs are located in neighboring genomic regions to protein-coding genes with established roles in mediating LXR effects on metabolism. Gene ontology analysis of protein-coding genes that were nearest to these lncRNAs showed enrichment for cholesterol metabolic processes, consistent with the idea that a subset of these non-coding RNAs may modulate the activity of adjacent protein-coding genes (Supplementary Table 2).

From the list of regulated lncRNAs in Supplementary Table 2, one of the most robustly induced hit that also showed evidence of LXR binding to its gene regulatory regions by LXR ChIP-seq studies [12] was a predicted transcript annotated as AI427809. We named this transcript MeXis (Macrophage-expressed LXR-induced sequence). Notably, the *MeXis* gene is located in close proximity to the established LXR target genes *Abca1* and *LeXis* [13] (Fig. 1a). Analysis of chromatin signatures from ENCODE indicated that *MeXis* and *Abca1* are distinct genes with separate promoters (Fig. 1a) [1415]. 5’ and 3’ rapid amplification of cDNA ends (RACE) experiments defined the MeXis transcript ends (Supplementary Fig. 2). RNA-copy number analysis showed that MeXis was highly expressed in murine macrophages (Supplementary Fig. 3a) and real-time PCR analysis showed that MeXis and *Abca1* expression was induced by LXR (GW3965) and RXR (LG268) agonists in primary macrophages in an LXR-dependent manner (Fig. 1b). MeXis expression was also induced in macrophages by physiologic lipid signals such as oxidized or acetylated LDL (Fig. 1c). In addition, oxysterol agonist of LXR induced MeXis expression in macrophages (Supplementary Fig. 3b). Intriguingly, MeXis showed a distinct pattern of LXR-dependent regulation compared to the lncRNA LeXis, which is expressed in liver but not macrophages (Fig. 1d) [13]. MeXis was also expressed in adipose tissue (Supplementary Fig. 3c).

MeXis is an LXR-responsive lncRNA that influences Abca1 expression

We identified an LXR-response element (LXRE) within the *MeXis* promoter region that was bound by LXRs in ChIP-seq analysis (Fig. 1e). In contrast to most of LXR target genes which are responsive to both LXRs, the *MeXis* promoter was bound by LXRβ but not LXRα. Consistent with this result, MeXis expression was induced by LXR activation in WT and *Lxra*$^{-/-}$ but not *Lxrb*$^{-/-}$ peritoneal macrophages, whereas *Abca1* expression was responsive to both LXRs (Fig. 1f and Supplementary Fig. 3d).To further explore isoform specific regulation of *MeXis*, we treated immortalized LXR DKO bone-marrow-derived macrophages (BMDMs), as well as LXR DKO BMDMs stably expressing LXRα, with GW3965. *Abca1* was induced with LXR activation in LXRα-expressing BMDMs but not in

DKO controls, whereas *MeXis* was not induced in either cell type (Supplementary Fig. 3e). These data further suggest that *MeXis* is an LXRβ-selective target gene.

Computational scores that distinguish protein-coding from non-coding RNAs predicted a low-coding potential for the MeXis transcript (Fig. 1g). Although the MeXis transcript does contain a number of short potential open-reading frames, we found no evidence of translation and production of a protein product from MeXis using a coupled *in vitro* transcription-translation assay (Supplementary Table 3 and Supplementary Fig. 4a). Single molecule RNA FISH in immortalized mouse bone-marrow derived macrophages confirmed nuclear localization of MeXis (Supplementary Fig. 4b). MeXis was predominantly located in the insoluble nuclear pellet enriched for chromatin, whereas the protein-coding *36b4* mRNA was predominantly present in cytoplasm (Supplementary Fig. 4c). Even when exogenously expressed at elevated levels, MeXis was predominantly nuclear (Supplementary Fig. 4d). This localization strongly suggests that MeXis most likely acts as a nuclear RNA, rather than being translated into a short protein in the cytoplasm.

Since some *lnc*RNAs have been shown to regulate the expression of adjacent genes [16,17], we hypothesized that loss of MeXis may impact the expression of *Abca1*. In support of this idea, siRNA-mediated knockdown of either MeXis or RXRα/β in mouse peritoneal macrophages decreased *Abca1* transcript levels (Fig. 2a). An antisense oligonucleotide (ASO) targeting MeXis also reduced *Abca1* levels (Supplementary Fig. 4e). Reciprocally, stable overexpression of MeXis in macrophages enhanced *Abca1* expression and cholesterol efflux capacity to ApoA-I acceptors (Fig. 2b, 2c, Supplementary Fig. 4f).

MeXis deficiency affects Abca1 expression, cholesterol efflux, and atherogenesis

To better decipher the contributions of MeXis to macrophage metabolism, we generated *MeXis*-knockout mice (Supplementary Fig. 5a). We used a strategy in which FLP excised the targeting cassette following homologous recombination, such that no extraneous promoter sequences were left behind after recombination. Consistent with our siRNA studies, $MeXis^{-/-}$ peritoneal macrophages showed decreased *Abca1* transcript levels (Fig. 2d). Notably, in western-diet fed mice, *Abca1* mRNA expression was differentially altered across tissues in $MeXis^{-/-}$ as compared to WT mice (Fig. 2d). For example, liver *Abca1* was not significantly different between groups, whereas heart and kidney *Abca1* expression was lower in $MeXis^{-/-}$ compared to WT mice (Fig. 2d). We also confirmed that Abca1 protein levels were reduced in $MeXis^{-/-}$ compared to WT macrophages (Fig. 2e). These results suggest that *MeXis* augments *Abca1* expression in a context-specific manner.

We observed minimal changes in expression of other LXR target genes in response to MeXis overexpression, knockdown or knockout (Supplementary Fig. 5b-d), suggesting that MeXis does not regulate all LXR target genes equivalently. Unbiased transcriptomic analysis of WT and $MeXis^{-/-}$ primary peritoneal macrophages showed enrichment for lipid metabolic pathways and inflammatory signaling (Supplementary Table. 4). Consistent with the alteration in *Abca1* expression in $MeXis^{-/-}$ macrophages, we observed a decrease in ApoA-I-dependent efflux capacity in peritoneal macrophages from $MeXis^{-/-}$ compared to WT mice (Fig. 2f, Supplementary Fig. 4g). By contrast, loss of MeXis in macrophages was not associated with a change in cholesterol uptake (Supplementary Fig. 4h). Furthermore,

compared to WT macrophages, *MeXis*$^{-/-}$ peritoneal macrophages showed higher cholesterol content *in vivo* in western-diet fed mice (Fig. 2g). Additionally, morphological "foam cell" formation, as assessed by oil-red O staining, was in *MeXis*$^{-/-}$ peritoneal macrophages (Fig 2h, Supplementary Fig. 4i). In accordance with the idea that MeXis primarily affects macrophage responses, there were no differences in serum cholesterol or triglyceride levels between *MeXis*$^{-/-}$ and WT mice, either when fed chow or western diet (Supplementary Fig. 6). Taken together, these results suggest that MeXis is required for maximal *Abca1* expression in the face of macrophage cholesterol loading.

To further explore the ability of MeXis to act as an RNA and to confirm its ability to modulate *Abca1* expression *in vivo*, we expressed MeXis in mouse liver using an adenoviral vector. Notably, we observed an increase in serum cholesterol levels—a hallmark feature of enhanced hepatic ABCA1 expression—in mice ectopically expressing MeXis in liver (Fig. 2i). We also confirmed that MeXis expression in liver induced *Abca1* mRNA without affecting the expression of other LXR target genes (Fig. 2j). ABCA1 protein levels were correspondingly increased by MeXis expression (Fig. 2k).

Cholesterol efflux capacity is an important determinant of atherosclerotic plaque development and progression. To examine the impact of MeXis on atherosclerosis, we reconstituted the bone marrow of irradiated *Ldlr*$^{-/-}$ mice with WT or *MeXis*$^{-/-}$ hematopoetic cells (Fig. 3a). Real-time PCR analysis of bone marrow from recipient mice collected at the time of sacrifice confirmed engraftment (Supplementary Fig. 7a). We found reduced *Abca1* expression and enhanced inflammatory gene expression in the bone marrow of mice transplanted with *MeXis*$^{-/-}$ bone marrow (Supplementary Fig. 7a). *En face* analysis of atherosclerotic plaque area after 17 weeks of western diet feeding showed markedly increased atherosclerotic burden in mice transplanted with *MeXis*$^{-/-}$ compared to WT bone marrow (Fig. 3a, 3b). No differences in plasma cholesterol or triglyceride levels were observed between the two groups (Supplementary Fig. 7b). Consistent results were obtained when we assessed atherosclerosis by quantification of oil-red O–stained aortic root sections (Fig 3c, 3d). Histological analysis showed larger lesions in *MeXis*$^{-/-}$ bone marrow-transplanted compared to WT bone marrow-transplanted mice, as well as increased staining for the macrophage-specific marker CD68 (Fig. 3e and Supplementary Fig. 7c). Laser-capture microdissection of CD68-positive cells revealed decreased expression of *Abca1* and *MeXis* in macrophages within atherosclerotic lesions from *MeXis*$^{-/-}$ bone marrow-compared to WT bone marrow-transplanted mice (Fig 3f,g). Taken together, these results demonstrate that macrophage *MeXis* expression is a determinant of susceptibility to atherosclerosis in mice.

MeXis interacts with DDX17 and modulates Abca1 transcription

eRNA expression can serve as a surrogate marker of enhancer site activity and transcriptional activation [18]. Enhancer elements surrounding *Abca1* in macrophages have been defined previously (Supplementary Fig. 8) [19]. Interestingly, *MeXis*$^{-/-}$ macrophages showed decreased eRNA expression from *Abca1* enhancers in response to LXR activation, as compared to WT cells (Fig. 4a). To assess whether MeXis can affect transcription of the *Abca1* gene in *trans*, we crossed *Abca1*$^{Flox/Flox}$ mice with heterozygous *MeXis*$^{-/+}$ mice.

This strategy enabled us to measure effects of *MeXis* deficiency specifically on the *Abca1* transcript that is *trans* to the mutant *MeXis* allele. We found that a reduction in MeXis expression reduced *Abca1* expression in *trans* (Fig. 4b, Supplementary Fig. 9a).

These observations led us to hypothesize that MeXis may influence chromatin dynamics at the *Abca1* locus, thereby modulating its transcription. Consistent with this idea, ATAC-seq performed on peritoneal macrophages showed blunted accessibility at multiple sites within the *Abca1* gene locus in the setting of *MeXis* deficiency (Fig. 4c). Quantification of accessible sites neighboring the *Abca1* promoter revealed decreased accessibility in *MeXis* $^{-/-}$ macrophages. By contrast, we found no difference in accessibility at the *Tlr4* locus (Fig. 4d), indicating selectivity of the effect of *MeXis* deficiency for certain chromatin regions. Genome-wide normalization revealed that the LXR target gene activation signature was largely preserved in *MeXis*-deficient macrophages; however, multiple sites within the *Abca1* locus showed differential accessibility between WT and *MeXis*$^{-/-}$ macrophages (Fig. 4e and Supplementary Fig. 9b). By contrast, the accessibility of very few sites was substantially altered at other LXR target gene loci (Supplementary Fig. 9c). Unbiased genome-wide analysis of differentially-accessible chromatin sites between WT and *MeXis*$^{-/-}$ macrophages showed enrichment for lipid transport and related processes (Supplementary Fig. 9d).

To further investigate the mechanism of *MeXis* action, we used an unbiased lncRNA:chromatin affinity capture technique [20] to pull down *MeXis* from macrophage extracts and identify interacting proteins (Supplementary Fig.10a). Analysis of the *MeXis* interactome by mass spectrometry identified DDX17, an established nuclear receptor coactivator[21,22], as a potential interacting partner (Supplementary Fig.10b).We confirmed a robust interaction between *MeXis* and DDX17 in RNA immunoprecipitation studies in mouse macrophages, either with or without the use of a cross-linking agent (Fig. 5a). The prior characterization of DDX17 as a transcriptional coactivator led us to hypothesize that DDX17 may serve this function at the *Abca1* locus. In line with this idea, ChIP-PCR analysis revealed that DDX17 was enriched at LXR binding sites in *Abca1* enhancer regions in macrophages (Fig 5b). Moreover, DDX17 binding was substantially reduced as a consequence of *MeXis* deletion (Fig. 5b). Interestingly, the pattern of LXR binding was also altered as a consequence of loss of *MeXis*, with reduced occupancy at the *Abca1* promoter, but enhanced binding at an intronic site (Fig. 5b). These results suggest that MeXis facilitates the coactivator actions of DDX17 to enhance LXR-mediated *Abca1* expression. To definitively determine if *MeXis* is recruited to the *Abca1* gene locus, we used ChIRP-qPCR. Using this technique, we found that *MeXis* bound to at a number of sites at *Abca1* that show differential accessibility between *MeXis*$^{-/-}$ and WT macrophages (Fig. 5c)

To further define the importance of DDX17 in *Abca1* regulation, we generated DDX17-deficient immortalized bone marrow-derived macrophages utilizing CRISPR-Cas editing (Supplementary Fig.10c). Deletion of DDX17 using two different excision strategies reduced *Abca1* levels at baseline and in response to LXR activation (Fig. 5d, e). These results strongly suggest that DDX17 is required for maximal *Abca1* expression in macrophages. To analyze the epistatic relationship between DDX17 and *MeXis*, we generated DDX17/*MeXis* double-knockout macrophages using CRISPR-Cas. Deletion of *MeXis* in the setting of DDX17 deficiency failed to further reduce *Abca1* transcript or

protein levels, as compared to DDX17 single knockout (Fig. 5f-g). Taken together, these results demonstrate that DDX17 contributes to MeXis-dependent regulation of *Abca1*.

Finally, we assessed whether the LXR-MeXis-*Abca1* pathway is operational in human cells. Genome-batch conversion between human and mouse genome builds revealed the genomic region surrounding the *MeXis*/Abca1 locus showed a degree of conservation between species (Supplementary Fig.11). A noncoding human RNA transcript in this region, identified as TCONS00016111, showed some sequence conservation with *MeXis* (Fig. 6a and Supplementary Fig.11). Intriguingly, TCONS00016111 expression was induced in response to LXR activation in human THP-1 macrophages (Fig 6b). Moreover, ASOs targeting TCONS00016111 reduced *ABCA1* transcript levels and ApoA-I-specific cholesterol efflux (Fig. 6c-d). Furthermore, lentiviral transduction of MeXis into *MeXis*$^{-/-}$ or THP-1 macrophages increased *ABCA1* expression (Fig. 6e, f).

Finally, GWAS from the CARDIOGRAM Plus consortium[23] identified a moderately significant association between a SNP overlapping the TCONS00016111 transcript and human coronary artery disease (P=4.78E–6) (Fig. 6g). These results support the notion that an LXR-lncRNA-*Abca1* axis is operational in humans and may have relevance for human disease.

Discussion

Previous work has identified important roles for eRNAs in regulating gene expression programs [24]. Our study expands the repertoire of noncoding RNA-mediated gene activation by showing that a lncRNA can help specify nuclear receptor regulatory circuits. Our results suggest that induction of MeXis expression in response to activation of LXRs augments *Abca1* expression and macrophage cholesterol efflux in a context-specific manner. It seems likely that MeXis may contribute to cell type-specific regulation of *Abca1* expression by LXRs. Our work, however, does not exclude the possibility that MeXis may have targets other than *Abca1*.

Our findings are consistent with previous reports that intergenic lncRNAs and their genomically-adjacent protein-coding genes tend to exhibit similar spatiotemporal expression profiles [2526]. Recent work suggests that at least some of the local effects of lncRNAs are the results of promoter activity and the act of transcription rather than lncRNA-specific features[11]. Although our results do not exclude the possibility that *cis* regulatory elements at the *MeXis* locus exert an influence on *Abca1* transcription, our data support that transcript-dependent actions also contribute to *Abca1* regulation.

This study also reveals an unexpected to role for a lncRNA in cardiovascular disease. Control of macrophage gene expression by the LXR pathway is causally linked to the pathogenesis of atherosclerosis. Identification of MeXis fills a gap in our understanding of pathways that control cellular responses to cholesterol overload and atherosclerosis.It is tempting to speculate that targeting the LXR-MeXis-*Abca1* axis may enhance macrophage reverse cholesterol transport to treat or prevent atherosclerotic disease while bypassing undesirable side effects of LXR activation in other tissues.

Materials & Methods

Reagents, Plasmids, and Gene Expression

GW3965 was synthesized as previously described[27]. LG268 was from Ligand Pharmaceuticals. Oxysterols were purchased from Sigma and used as described[28]. Simvastatin sodium salt was from Calbiochem. Ligands were dissolved in dimethyl sulfoxide before use in cell culture. MeXis was amplified from RNA purified from GW3695-treated primary mouse peritoneal macrophages using KOD polymerase (Millipore), forward 5'GTCTGAAAAGGAAGTTGAAGAAGA3' and reverse 5' AAGGAATCTAGTAAATTTTAATACTAA3' primers. Primers were designed to provide flanking *attB* sequences and a *SacI* site at the immediate 3' end. For details of oligonucleotide sequences please see supplementary file number 12. The fragments were then cloned into pDONR221 using the Gateway system and the minimal SV40 polyadenylation sequence was inserted at the *SacI* site. ON-Targetplus siRNAs (Catalog number R-050345) were used with Dharmafect 4 reagent per the manufacturer's recommendations for knockdown studies (Dharmacon). For gene expression analysis, RNA was isolated using TRIzol reagent (Invitrogen) and analyzed by real-time PCR using an Applied Biosystems 7900HT sequence detector or Applied Biosystems Quant Studio 6 Flex. Results are normalized to 36B4 or cyclophilin. The following antibodies were used for immunohistochemistry: CD68 (MCA1957GA, AbD) 1:400 with secondary antibody biotin-SP-conjugated AffiniPure goat anti-rat IgG (H+L) (Jackson Laboratories). Details of antibodies and full-length blots are provided in supplementary file 13 and 14. In brief, for immunoblot analysis, the following antibodies were used: ABCA1 (Novus) 1:1,000, and actin (Sigma) 1:10,000.. For ChIP analysis, we used the LXR antibody previously described[29]; DDX17 antibody was generated by Douglas Black, UCLA[30]. plentiCRISPR v2 was used for lentivrius production; the guide RNA was inserted into Bsmb1-digested plasmid and the plasmid was ligated with T4 DNA ligase. Guide insertions were verified via sequencing.For lentiviral overexpression studies, MeXis was cloned into the pSLIK-Zeo vector system [31] and modified for lncRNA expression by replacement of the sequence between NcoI and MfeI sites in the pEN_TT entry vector with a minimal SV40 polyadenylation signal. The MeXis sequence was inserted into the NcoI site immediately upstream of the polyadenylation signal. Lentiviruses were packaged and purified as described [32]. For retroviral and adenoviral expression, the MeXis sequence was transferred from the pEN-TTpA entry vector to pBABE and pAd/CMV/V5-DEST, respectively, using the Gateway cloning system (Invitrogen Life Technologies).

Animals and diets

Mice were housed in a temperature-controlled room under a 12-hour light/12-hour dark cycle and under pathogen-free conditions. Experiments used 12 week- old male mice unless otherwise specified. Age-matched male *Ldlr*$^{-/-}$ mice on C57BL/6 background were purchased from Jackson Laboratories (catalog number 2207). Mice lacking LXRα and/or LXRβ were originally provided by David Mangelsdorf, University of Texas Southwestern Medical Center, Dallas, Texas, USA[33] and were backcrossed to on C57BL/6 background for more than 10 generations. *MeXis* global knockout mice on a C57BL/6 background were generated at UCDavis Knockout Mouse Project (KOMP) using the strategy outlined in

supplemental figure 5. *Abca1*$^{flox/flox}$ mice on a C57BL/6 background were obtained from John Parks, Wake Forest University[34]. Mice were fed a chow diet except as indicated, where mice were placed on a Western diet (21 percent fat, 0.21 percent cholesterol; D12079B; Research Diets Inc.). We measured cholesterol and triglycerides as previously described[13]. At the time of sacrifice, tissues and blood were collected by cardiac-puncture and immediately frozen in liquid nitrogen and stored at – 80°. For adenoviral infections, age-matched male mice were injected with 2.0×10^9 PFU by tail-vein injection and were sacrificed six days later following a six-hour fast. Tissue was processed for isolation of RNA as above. All animal experiments were approved by the UCLA Institutional Animal Care and Research Advisory Committee and performed in strict accordance with the recommendations in the Guide for the Care and Use of Laboratory Animals of the National Institutes of Health.

Cell culture

Primary peritoneal macrophages were isolated four days after thioglycollate injection and prepared as described[27]. Mouse primary hepatocytes were isolated as previously described and cultured in William's E medium with 5 percent FBS[27]. Peritoneal cells were incubated in 0.5-10 percent FBS in DMEM, with or without 5 μM simvastatin and 100 μM mevalonic acid (EMD Biosciences). Five to eight hours later, cells were pretreated with DMSO or appropriate ligand overnight. The *in vitro* translation assay was performed using the TnT Coupled Transcription/Translation System (PROMEGA) according to the manufacturer's protocol.THP-1 cells from ATCC were treated were treated with custom siRNA from Dharmacon (50 nM) and harvested 36 h later. Modified gapmer ASOs were obtained from IDT and used with Dharmafect 4 or Attractene transection reagent at a final concentration of 50 nM. THP-1 cells were differentiated with phorbol 12-myristate 13-acetate (PMA) at 10 ng/ml followed by GW3965 treatment. Immortalization of bone marrow-derived macrophages (iBMDMs)to generate stable cell lines was performed as previously described[34]. These stable cell lines were obtained via puromycin selection of lentivirus-treated cells starting from a single clonal population. Gene expression or western blot results are shown for a pool of selected cells unless otherwise noted. All cell lines were tested for mycoplasma contamination. Subcellular RNA fractions were obtained according to the protocol of Bhatt *et al.*[31] and as we previously described [13,35].

Cholesterol efflux and uptake

Assays were performed as previously described [27]. Briefly, peritoneal macrophages from WT or *MeXis*$^{-/-}$ mice were labeled with [^{3}H]cholesterol (1.0 μCi/ml) (Perkin Elmer) in the presence of acyl-CoA:cholesterol O-acyltransferase inhibitor (2 μg/ml)followed by treatment with DMSO or LXR(1 μM GW3965). After equilibration of the cholesterol pools and washing, cells were incubated in DMEM containing 0.2% BSA in the absence or presence of apoA-I (Meridian Life Sciences) (15 μg/ml) or HDL purchased from Lee Biosolutions (Catalog number 361-10-0.01) (50 μg/ml) for 6 h. The data are presented as percent apoA-I- or HDL-specific efflux. For uptake assays, resident mouse peritoneal mouse macrophages were obtained from age-matched WT and *MeXis*$^{-/-}$ mice. Peritoneal macrophages were suspended in starvation media (1% Lipoprotein Deficient Serum (LPDS), simvastatin, mevalonic acid) and incubated at 37° C for 16 hours. Cells were then treated with DiI-

acetyl-LDL (Invitrogen) at concentrations of 0 μg/ml, 50 μg/ml and 100 μg/ml and incubated at 37 ° C for an additional 4 h. After the 4 h incubation period, cells were washed three times with PBS containing bovine serum albumin (2mg/ml), harvested, and lysed in RIPA buffer. To measure the uptake of DiI-acetyl-LDL by peritoneal macrophages, cell lysates were analyzed for fluorescence using a Clario Star plate reader with an excitation of 554 nm and an emission of 571 nm. Values for fluorescent intensity were normalized to total protein concentration and displayed relative to the untreated group.

Atherosclerosis analysis

Immunohistochemistry of sections and preparation and staining of frozen and paraffin-embedded sections from aortas were performed as described previously [36]. Atherosclerosis in the aortic roots and the descending aortas (*en face*) were quantified by computer-assisted image analysis as described [37]. Atherosclerotic lesions at the aortic valve were analyzed as described [27]. Laser capture microdissection was used as previously outlined [38], except that an LMD7000 Laser Microdissection System (Leica) was used at the UCLA Advanced Microscope CNSI core lab. The Arcturus PicoPure RNA Isolation Kit (Applied Biosystems) was used for RNA processing and amplification.

RACE

The 5’ and 3’ ends of the MeXis transcript were defined using mouse peritoneal macrophage RNA and the FirstChoice RLM-RACE kit (Ambion) according to manufacturer’s protocol, with modifications. Briefly, for 5’ RACE, degraded mRNA 5’ ends were dephosphorylated with CIP and then full-length mRNA was decapped with TAP. Following 5’RACE adapter ligation, reverse transcription was performed using the SuperScriptIII First-Strand Synthesis system (Invitrogen) and MeXis-specific primers. For 3’ RACE, RNA was reverse transcribed using SuperScriptIII First-Strand Synthesis system (Invitrogen) and adapter-linked oligo dTs. The resulting cDNA was amplified by nested PCR across a 55-65 °C melting temperature gradient using KOD polymerase (Millipore), with the inner primers containing *att*B sequences. Aliquots of reactions were inspected on 1% agarose gels for product size and abundance. Products of selected PCR reactions were purified using the NucleoSpin Gel and PCR Cleanup kit (Clontech) and were inserted into pDONR221 by Gateway cloning procedures. Cloned fragments were sequenced and then aligned to the mouse genome with the BLAST analysis tool. RNA fractionation assays were done as previously described [13].

RNA Sequencing

RNA sequencing libraries were constructed with the TruSeq RNA Sample Prep Kits (Illumina) on RNA isolated from peritoneal macrophages treated with or without GW3965. Samples were indexed with adapters and submitted for paired-end 2 × 100-bp sequencing using an Illumina HiSeq2000 instrument. RNA-seq reads were aligned with TopHatv2.0.2 to the mouse genome, version mm9[39]. Transcripts were assessed and quantities were determined by Cufflinks v2.0.2, using a GTF file based on Ensembl mouse NCBI37. Comparisons of expression levels were made using FPKM values using Cuffdiff from the Cufflinks package [40]. In order to analyze lncRNA expression in more depth, we built a comprehensive, non-redundant mouse gene database by merging the Gencode and Noncode

annotations. Reads were aligned to the mouse genome (GRC38/mm10 assembly) using STAR[41]. Gene-level count summaries were estimated with HTSeq. We employed a comprehensive, non-redundant mm10 genome annotation that incorporates protein and lncRNA genes from Gencode and lncRNA annotations from Noncode v4 [42]. Coding potential scores for each transcript in the merged annotation were estimated with CPAT [43]. In addition, we used CNCI as another method to classify coding potential of sequences of interest [44]. Gene-level expression estimates in units of FPKMs were computed in-house as above. For downstream analysis, the following entries were masked: 1) genes with no counts, 2) genes with low (<50bp) nucleotide sequence uniqueness, and 3) Gencode biotypes other than protein coding or lncRNA. The final genome annotation we employed for downstream analyses comprised 50,608 genes (21098 protein-coding, 29510 lncRNA). Expression fold changes after GW treatment were estimated from FPKM ratios. Enrichment analyses on the set of up-regulated coding and non-coding genes included pathways analyses with MetaScape and *cis*-regulatory region enrichment with default parameters in GREAT [45].

Lipid analysis

Cellular lipid content was obtained using a Folch extraction. Briefly, chloroform extracts were dried under nitrogen and solubilized in water. Tissue and serum cholesterol and triglycerides were determined using a commercially available enzymatic kit (Wako). Mice were fasted for at least 6 hours prior to blood collection and sacrifice.

ChIP

ChIP studies were performed as described elsewhere [13]. Briefly primary mouse peritoneal macrophages (approximately 40 million per sample) were cross-linked using a final formaldehyde concentration of 1% at room temperature for 10 minutes. The reaction was quenched with the addition of glycine. Sonicated chromatin isolated with lysis buffer (50 mM HEPES-KOH, pH 7.5, 140 mM NaCl, 1 mM EDTA, 10% glycerol, 0.5% NP-40, 0.25% Triton X-100)was incubated overnight at 4°C with control IgG or 2.5 ug per ml of lysate of anti-LXR (previously generated by JaKobsson et al from Karolinska Institute)[29], or anti-DDX17 antibody (gift of Douglas Black, UCLA). Protein A Dynabeads (Invitrogen) were added for 4 hours. Washing, reverse crosslinking and sample elution were performed as previously outlined [13]. Chip-seq for LXR isoforms was done using Flag-tagged LXRα or LXRβ in iBMDM cell lines[34]. Macrophages (12×10^6) were crosslinked using a double fixation protocol with 2 mM disuccinimidyl glutarate for 30 min and 1% methanol-free ultrapure formaldehyde for 10 min before quenching with 2 M glycine. Cells were lysed with RIPA buffer and, after chromatin shearing by sonication using a Bioruptor (Diagenode) apparatus, incubated overnight with protein G magnetic Dynabeads (Invitrogen) coupled with 3 μg of either anti-FLAG M2 (SIGMA #F3165) or anti-H3K27ac (Abcam #ab4729) antibodies. Immunoprecipitated DNA was purified using Qiagen purification kit (Qiagen #28144). For high-throughput sequencing, a minimum of 10 ng of DNA was obtained by pooling DNA from 10 independent ChIP preparations (for FLAG-LXR sequencing) or 6 different ChIP preparations (for H3K27ac sequencing). DNA was then used for library preparation and subsequent Illumina HiSeq sequencing by the Centre de Regulació Genomica (CRG, Barcelona, Spain) genome facility. The primary data have been deposited to GEO, accession number GSE104027.

Fluorescent RNA FISH

Custom design RNAscope probes against *MeXis* were prepared and obtained from Advanced Cell Diagnostics (Catalog number 495011). *MeXis* was visualized in immortalized mouse bone-marrow derived macrophages using an RNAscope assay and the Multiplex Fluorescent Reagent Kit V2, following the manufacturer's recommended protocol with use of a HybEZ oven (Advanced Cell Diagnostics); however, we used a protease dilution of 1:5 instead of 1:30.

RNA immunoprecipitation

We followed the protocol outlined by Tsai and colleagues[46]. Briefly cellular extracts from native or cross-linked (1% formaldehyde) primary peritoneal macrophages were treated with DNASE I followed by incubation with DDX17 antibody or IgG control overnight. Complexes were captured using Dynabead Protein G (Life technologies) and RNA was eluted using the RNeasy micro kit (Qiagen).

Microarrays

cDNA microarray analysis was performed for primary peritoneal macrophages treated with GW3695. Transcriptional profiling was performed at the University of California, Los Angeles, TCGB core facility using the Agilent SurePrint G3 Gene Expression array. Data were analyzed using GeneSpring software (Agilent Technologies) and DAVID Functional Analysis Tools [47]. Data available at GSE107977.

ChIRP

Chirp was performed as described[20] with a few modifications. First, cross-linking of RAW264.7 cells from ATCC treated with GW3965 was done using 3% formaldehyde. Second, we used a longer probe design algorithm (~50 bp instead of recommended 20 bp) that optimized the signal-to-noise ratio and *MeXis* retrieval, as determined using pilot experiments comparing shorter and longer probe sets performed with RNAase and DNAase controls. For ChIRP-MS, the final protein elution was done in a solution of 50 mM triethyl ammonium bicarbonate, 12 mM sodium lauryl sarcosine, and 0.5% sodium deoxycholate.

ATAC-Seq

Peritoneal macrophages were isolated and treated for 3 hours with or without GW3965. Using four replicates per condition, libraries were prepared using the Nextera Tn5 Transposase kit (Illumina) as described[48] with slight modifications. Libraries were single-end sequenced (50bp) on an Illumina HiSeq 2000 instrument. Reads were mapped to the mouse genome (NCBI37/mm9) using Bowtie2, and were removed from the subsequent analysis if they were duplicated, mapped to mitochondrial genome, or aligned to unmapped contiguous sequences. Peak calling was performed using MACS2 using parameters callpeak --nomodel -g mm --keep-dup all -q .01 --llocal 10000. Overlapping peaks were merged together and used as probes for quantifying reads. The reads were converted to reads per million (RPKM) by dividing by the total number of reads within a peak divided by the peak length per million mapped reads. The average RPKM from four replicates was used to quantify the accessibility across all called peaks. Significance was determined by the

DESeq2 package in R Bioconductor[49]. P-values were adjusted using the Benjamini-Hochberg procedure of multiple hypothesis testing [50].

Statistical analysis

A non-paired student *t*-test was used to determine statistical significance, defined at P-value < 0.05. For multiple group experiments, ANOVA was used followed by multiple group analysis. Unless otherwise noted, error bars represent standard deviations. Except as noted in figure legends experiments were independently performed twice. Sample size is based on statistical analysis of variance and prior experience with similar *in vivo* studies.

Supplementary Material

Refer to Web version on PubMed Central for supplementary material.

Acknowledgments

We thank members of the Tontonoz, Smale, Black, and Nagy laboratories and the UCLA Atherosclerosis Research Unit for technical assistance and useful discussions. This work was support by NIH grants HL030568, HL066088, HL128822, Burroughs Wellcome Fund Career Award for Medical Scientists and UCLA Cardiovascular Discovery Fund (Lauren B. Leichtman and Arthur E. Levine Investigator Award).

References

1. Rohatgi A, et al. HDL cholesterol efflux capacity and incident cardiovascular events. The New England journal of medicine. 2014; 371:2383–2393. DOI: 10.1056/NEJMoa1409065 [PubMed: 25404125]
2. de la Llera-Moya M, et al. The ability to promote efflux via ABCA1 determines the capacity of serum specimens with similar high-density lipoprotein cholesterol to remove cholesterol from macrophages. Arteriosclerosis, thrombosis, and vascular biology. 2010; 30:796–801. DOI: 10.1161/ATVBAHA.109.199158
3. Libby P, Ridker PM, Hansson GK. Leducq Transatlantic Network on, A. Inflammation in atherosclerosis: from pathophysiology to practice. Journal of the American College of Cardiology. 2009; 54:2129–2138. DOI: 10.1016/j.jacc.2009.09.009 [PubMed: 19942084]
4. Cao Q, et al. The central role of EED in the orchestration of polycomb group complexes. Nature communications. 2014; 5:3127.
5. Zelcer N, Tontonoz P. Liver X receptors as integrators of metabolic and inflammatory signaling. The Journal of clinical investigation. 2006; 116:607–614. DOI: 10.1172/JCI27883 [PubMed: 16511593]
6. Bodzioch M, et al. The gene encoding ATP-binding cassette transporter 1 is mutated in Tangier disease. Nature genetics. 1999; 22:347–351. DOI: 10.1038/11914 [PubMed: 10431237]
7. Rust S, et al. Tangier disease is caused by mutations in the gene encoding ATP-binding cassette transporter 1. Nature genetics. 1999; 22:352–355. DOI: 10.1038/11921 [PubMed: 10431238]
8. Rinn JL, Chang HY. Genome regulation by long noncoding RNAs. Annual review of biochemistry. 2012; 81:145–166. DOI: 10.1146/annurev-biochem-051410-092902
9. Wang KC, et al. A long noncoding RNA maintains active chromatin to coordinate homeotic gene expression. Nature. 2011; 472:120–124. DOI: 10.1038/nature09819 [PubMed: 21423168]
10. Kotzin JJ, et al. The long non-coding RNA Morrbid regulates Bim and short-lived myeloid cell lifespan. Nature. 2016; 537:239–243. DOI: 10.1038/nature19346 [PubMed: 27525555]
11. Engreitz JM, et al. Local regulation of gene expression by lncRNA promoters, transcription and splicing. Nature. 2016; 539:452–455. DOI: 10.1038/nature20149 [PubMed: 27783602]
12. Zhang L, et al. Inhibition of cholesterol biosynthesis through RNF145-dependent ubiquitination of SCAP. eLife. 2017; 6

13. Sallam T, et al. Feedback modulation of cholesterol metabolism by the lipid-responsive non-coding RNA LeXis. Nature. 2016; 534:124–128. DOI: 10.1038/nature17674 [PubMed: 27251289]
14. Creyghton MP, et al. Histone H3K27ac separates active from poised enhancers and predicts developmental state. P Natl Acad Sci USA. 2010; 107:21931–21936. DOI: 10.1073/pnas.1016071107
15. Consortium EP. An integrated encyclopedia of DNA elements in the human genome. Nature. 2012; 489:57–74. DOI: 10.1038/nature11247 [PubMed: 22955616]
16. Quinn JJ, Chang HY. Unique features of long non-coding RNA biogenesis and function. Nature reviews Genetics. 2016; 17:47–62. DOI: 10.1038/nrg.2015.10
17. Huarte M, et al. A large intergenic noncoding RNA induced by p53 mediates global gene repression in the p53 response. Cell. 2010; 142:409–419. DOI: 10.1016/j.cell.2010.06.040 [PubMed: 20673990]
18. Cheng JH, Pan DZ, Tsai ZT, Tsai HK. Genome-wide analysis of enhancer RNA in gene regulation across 12 mouse tissues. Scientific reports. 2015; 5:12648. [PubMed: 26219400]
19. Daniel B, et al. The active enhancer network operated by liganded RXR supports angiogenic activity in macrophages. Genes & development. 2014; 28:1562–1577. DOI: 10.1101/gad.242685.114 [PubMed: 25030696]
20. Chu C, et al. Systematic discovery of Xist RNA binding proteins. Cell. 2015; 161:404–416. DOI: 10.1016/j.cell.2015.03.025 [PubMed: 25843628]
21. Auboeuf D, Honig A, Berget SM, O'Malley BW. Coordinate regulation of transcription and splicing by steroid receptor coregulators. Science. 2002; 298:416–419. DOI: 10.1126/science.1073734 [PubMed: 12376702]
22. Wortham NC, et al. The DEAD-box protein p72 regulates ERalpha-/oestrogen-dependent transcription and cell growth, and is associated with improved survival in ERalpha-positive breast cancer. Oncogene. 2009; 28:4053–4064. DOI: 10.1038/onc.2009.261 [PubMed: 19718048]
23. Nikpay M, et al. A comprehensive 1,000 Genomes-based genome-wide association meta-analysis of coronary artery disease. Nature genetics. 2015; 47:1121–1130. DOI: 10.1038/ng.3396 [PubMed: 26343387]
24. Li W, et al. Functional roles of enhancer RNAs for oestrogen-dependent transcriptional activation. Nature. 2013; 498:516–520. DOI: 10.1038/nature12210 [PubMed: 23728302]
25. Wang KC, Chang HY. Molecular mechanisms of long noncoding RNAs. Molecular cell. 2011; 43:904–914. DOI: 10.1016/j.molcel.2011.08.018 [PubMed: 21925379]
26. Khalil AM, et al. Many human large intergenic noncoding RNAs associate with chromatin-modifying complexes and affect gene expression. Proceedings of the National Academy of Sciences of the United States of America. 2009; 106:11667–11672. DOI: 10.1073/pnas.0904715106 [PubMed: 19571010]
27. Sallam T. The macrophage LBP gene is an LXR target that promotes macrophage survival and atherosclerosis. Journal of lipid research. 2014; 55:1120–1130. DOI: 10.1194/jlr.M047548 [PubMed: 24671012]
28. Rong X, et al. LXRs regulate ER stress and inflammation through dynamic modulation of membrane phospholipid composition. Cell metabolism. 2013; 18:685–697. DOI: 10.1016/j.cmet.2013.10.002 [PubMed: 24206663]
29. Jakobsson T, et al. GPS2 is required for cholesterol efflux by triggering histone demethylation, LXR recruitment, and coregulator assembly at the ABCG1 locus. Molecular cell. 2009; 34:510–518. DOI: 10.1016/j.molcel.2009.05.006 [PubMed: 19481530]
30. Wongpalee SP, et al. Large-scale remodeling of a repressed exon ribonucleoprotein to an exon definition complex active for splicing. eLife. 2016; 5
31. Shin KJ, et al. A single lentiviral vector platform for microRNA-based conditional RNA interference and coordinated transgene expression. Proceedings of the National Academy of Sciences of the United States of America. 2006; 103:13759–13764. DOI: 10.1073/pnas.0606179103 [PubMed: 16945906]
32. Boyden ES, Zhang F, Bamberg E, Nagel G, Deisseroth K. Millisecond-timescale, genetically targeted optical control of neural activity. Nature neuroscience. 2005; 8:1263–1268. DOI: 10.1038/nn1525 [PubMed: 16116447]

33. Peet DJ, et al. Cholesterol and bile acid metabolism are impaired in mice lacking the nuclear oxysterol receptor LXR alpha. Cell. 1998; 93:693–704. [PubMed: 9630215]
34. Ito A, et al. LXRs link metabolism to inflammation through Abca1-dependent regulation of membrane composition and TLR signaling. eLife. 2015; 4:e08009. [PubMed: 26173179]
35. Bhatt DM, et al. Transcript dynamics of proinflammatory genes revealed by sequence analysis of subcellular RNA fractions. Cell. 2012; 150:279–290. DOI: 10.1016/j.cell.2012.05.043 [PubMed: 22817891]
36. Bradley MN, et al. Ligand activation of LXR beta reverses atherosclerosis and cellular cholesterol overload in mice lacking LXR alpha and apoE. The Journal of clinical investigation. 2007; 117:2337–2346. DOI: 10.1172/JCI31909 [PubMed: 17657314]
37. Tangirala RK, Rubin EM, Palinski W. Quantitation of atherosclerosis in murine models: correlation between lesions in the aortic origin and in the entire aorta, and differences in the extent of lesions between sexes in LDL receptor-deficient and apolipoprotein E-deficient mice. Journal of lipid research. 1995; 36:2320–2328. [PubMed: 8656070]
38. Feig JE, Fisher EA. Laser capture microdissection for analysis of macrophage gene expression from atherosclerotic lesions. Methods in molecular biology. 2013; 1027:123–135. DOI: 10.1007/978-1-60327-369-5_5 [PubMed: 23912984]
39. Trapnell C, Pachter L, Salzberg SL. TopHat: discovering splice junctions with RNA-Seq. Bioinformatics. 2009; 25:1105–1111. DOI: 10.1093/bioinformatics/btp120 [PubMed: 19289445]
40. Trapnell C, et al. Transcript assembly and quantification by RNA-Seq reveals unannotated transcripts and isoform switching during cell differentiation. Nature biotechnology. 2010; 28:511–515. DOI: 10.1038/nbt.1621
41. Dobin A, et al. STAR: ultrafast universal RNA-seq aligner. Bioinformatics. 2013; 29:15–21. DOI: 10.1093/bioinformatics/bts635 [PubMed: 23104886]
42. Zhao Y, et al. NONCODE 2016: an informative and valuable data source of long non-coding RNAs. Nucleic acids research. 2016; 44:D203–208. DOI: 10.1093/nar/gkv1252 [PubMed: 26586799]
43. Koeth RA, et al. Intestinal microbiota metabolism of L-carnitine, a nutrient in red meat, promotes atherosclerosis. Nature medicine. 2013; 19:576–585. DOI: 10.1038/nm.3145
44. Sun L, et al. Utilizing sequence intrinsic composition to classify protein-coding and long non-coding transcripts. Nucleic acids research. 2013; 41:e166. [PubMed: 23892401]
45. McLean CY, et al. GREAT improves functional interpretation of cis-regulatory regions. Nature biotechnology. 2010; 28:495–501. DOI: 10.1038/nbt.1630
46. Tsai MC, et al. Long noncoding RNA as modular scaffold of histone modification complexes. Science. 2010; 329:689–693. DOI: 10.1126/science.1192002 [PubMed: 20616235]
47. Huang da W, Sherman BT, Lempicki RA. Systematic and integrative analysis of large gene lists using DAVID bioinformatics resources. Nature protocols. 2009; 4:44–57. DOI: 10.1038/nprot.2008.211 [PubMed: 19131956]
48. Buenrostro JD, Giresi PG, Zaba LC, Chang HY, Greenleaf WJ. Transposition of native chromatin for fast and sensitive epigenomic profiling of open chromatin, DNA-binding proteins and nucleosome position. Nature methods. 2013; 10:1213–1218. DOI: 10.1038/nmeth.2688 [PubMed: 24097267]
49. Soneson C, Love MI, Robinson MD. Differential analyses for RNA-seq: transcript-level estimates improve gene-level inferences. F1000Research. 2015; 4:1521. [PubMed: 26925227]
50. Benjamini Y, Hochberg Y. Controlling the False Discovery Rate - a Practical and Powerful Approach to Multiple Testing. J Roy Stat Soc B Met. 1995; 57:289–300.

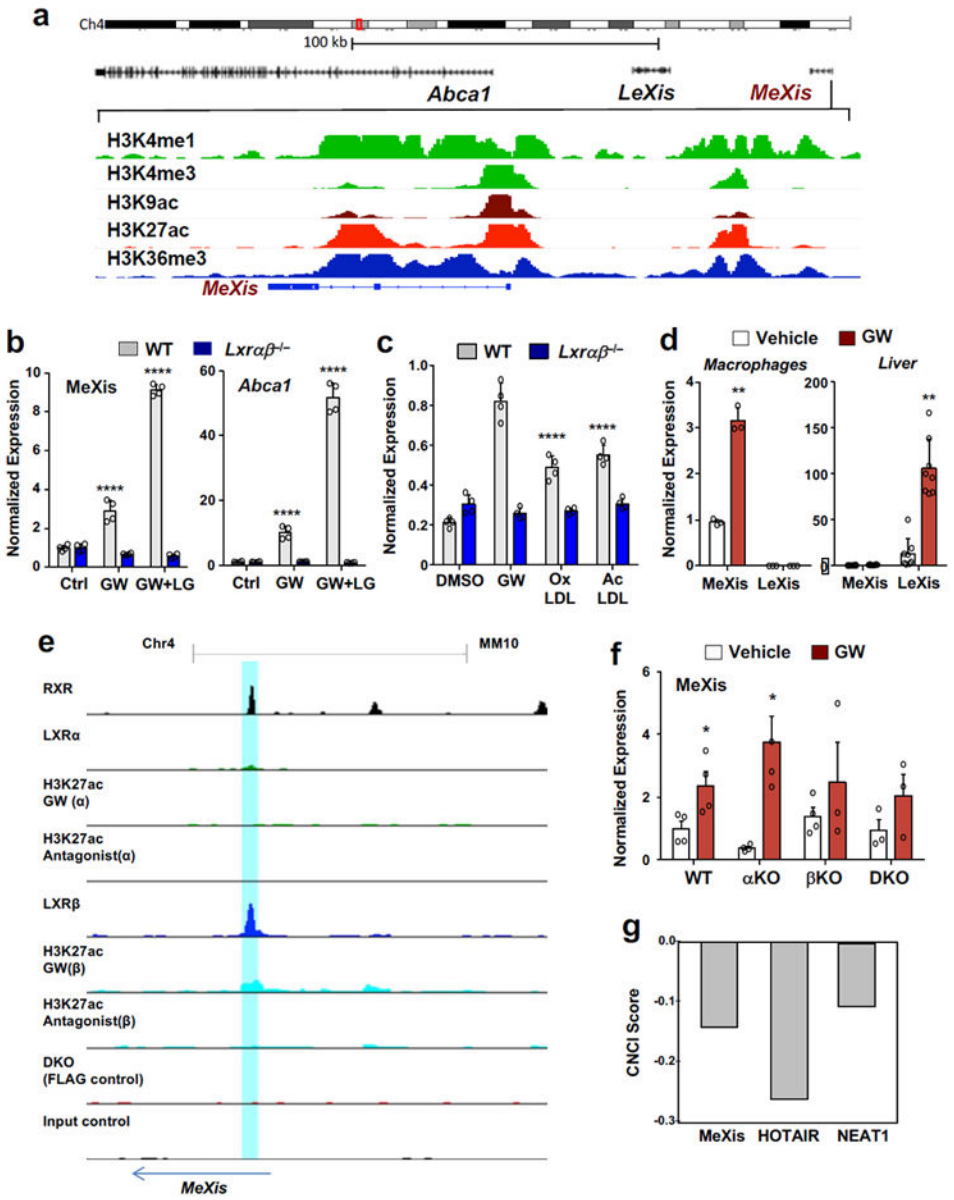

Figure 1. Regulation of the non-coding RNA *MeXis* by LXR

A. Schematic representation of the *MeXis* gene locus on the Integrative Genome Viewer (IGV) (top) and histone marks from LICR ENCODE data in the immediate region of the *MeXis* gene (bottom). **B.** Real-time PCR analysis of MeXis and *Abca1* expression in primary mouse macrophages treated with vehicle (Ctrl), GW3965 (GW, 0.5 μM) and/or the RXR ligand LG268 (LG, 50 nM). Results are representative of four independent experiments. Values are means ± SD. **** P<0.0001 by Two-way ANOVA followed by multiple comparisons test (Dunnett's). **C.** Real-time PCR analysis of MeXis expression in primary mouse macrophages treated with vehicle (Ctrl), GW3965 (GW, 0.5 μM) , oxidized LDL (oxLDL, 50 μg/ml), or acetylated LDL (acLDL, 50 μg/ml). Results are representative of four independent experiments. Values are means ± SD. **** P<0.0001 by Two-way ANOVA followed by multiple comparisons test (Dunnett's). **D.** Real-time PCR analysis of

MeXis and LeXis expression in primary mouse macrophages treated with vehicle or GW3965 (GW, 0.5 μM) (n = 3/group) or in liver harvested from WT mice treated with vehicle or GW3965 (40 mg/kg, by gavage) for 3 consecutive days (n = 8/group). Values are means ± SD. **E**. Chip-Seq analysis of LXR binding at the *MeXis* gene locus.Chip for LXRα and LXRβ in 3xFLAG-LXRα and 3xFLAG-LXRβ expressing immortalized bone marrow macrophage cell using FLAG, RXR and H3K27ac antibody. Cells treated with LXR agonist (GW3965, 1uM) and antagonist (GW2033, 1uM) shown. Blue shaded bar highlighting binding of LXR /RXR at *MeXis*.**F.** Real-time PCR analysis of MeXis expression in primary mouse macrophages from mice of the indicated genotypes treated with vehicle or GW3965 (GW, 0.5 μM). N=(4 for WT, αKO, βKO vehicle and 3 for DKO & βKO GW). Experiment repeated once with similar results. Values are means ± SEM. * $P<0.05$ by two-sided student's t-test. **G.** Prediction of coding potential of the indicated lncRNAs using Coding-Non-Coding Index (CNCI) software. A negative value indicates low coding potential.

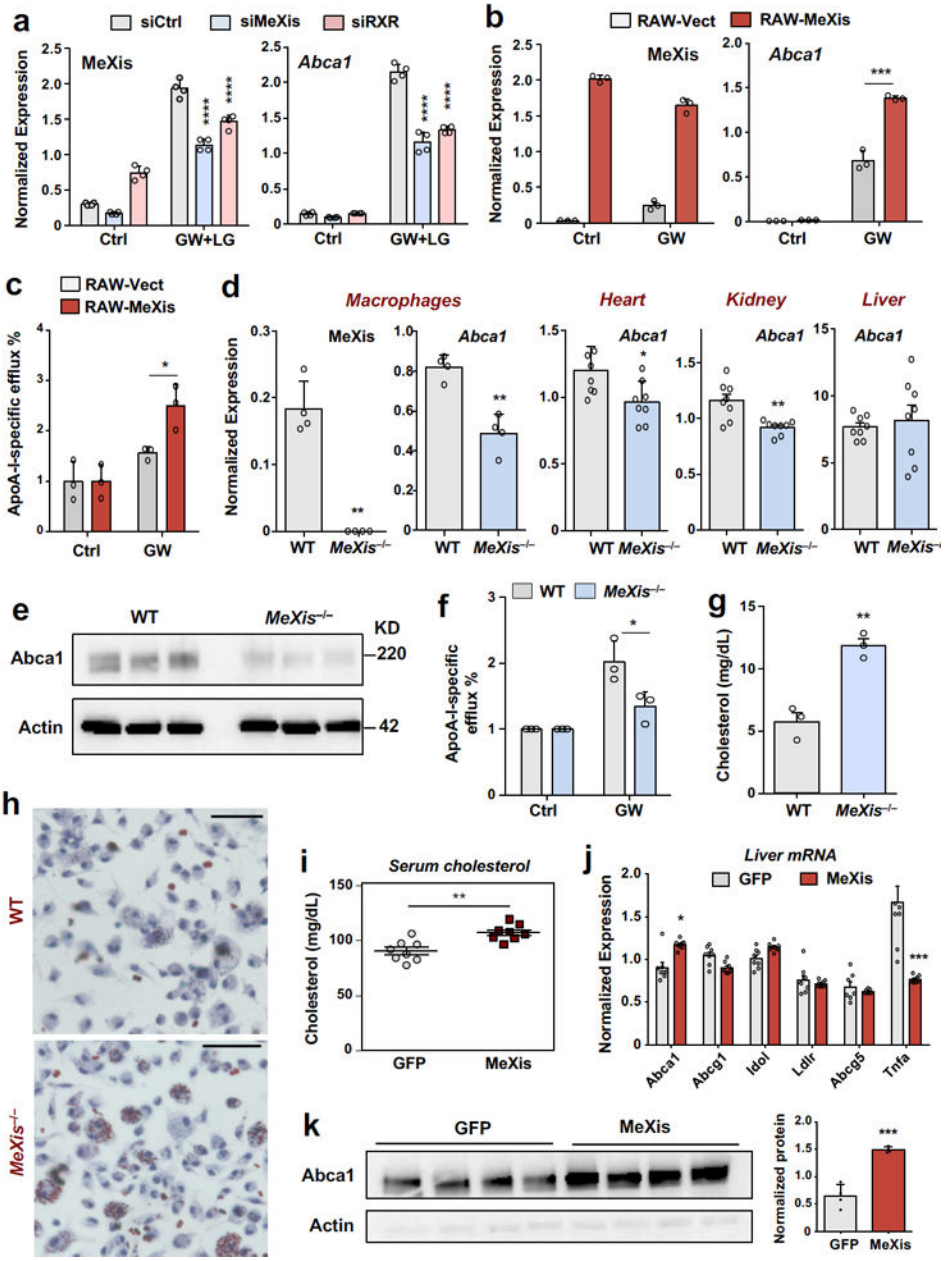

Figure 2. MeXis regulates *Abca1* expression and function

A. Real-time PCR analysis of MeXis and *Abca1* expression from primary macrophages treated with the indicated siRNAs (50 nM) followed by either vehicle (Ctrl) or a combination of GW3965 (GW, 0.5 μM) and the RXR ligand LG268 (LG, 50 nM) for 36 h. Results are representative of four independent experiments. Values are means ± SD.**** P<0.0001 by Two-way ANOVA followed by multiple comparisons test (Sidak's). **B.** Real-time PCR analysis of MeXis and *Abca1* expression 10 days after stable overexpression of control vector (Vect) or MeXis in RAW cells treated with vehicle (Ctrl) or GW3965 (GW, 0.5 μM). Results are representative of three independent experiments. Values are means ± SD.*** P < 0.001 by two-sided student's t-test. **C.** Cholesterol efflux in the presence of

ApoA-I from RAW macrophages loaded with [^{3}H]cholesterol (1.0 μCi/ml) and treated with the acyl-CoA:cholesterol O-acyltransferase inhibitor (2 μg/ml) and either with DMSO or LXR ligand (1 μM GW3965). ApoA-I-specific efflux represents percent radiolabelled cholesterol efflux in the presence of ApoA-I normalized to DMSO. Experiments were conducted in triplicate. Data are expressed as mean ± SD.* P<0.05 by two-sided student's t-test.**D.** Real-time PCR analysis of MeXis and *Abca1* expression in primary mouse macrophages (results are representative of four independent experiments; values are means ± SD) and of *Abca1* expression in heart, kidney and liver of mice fed a western diet for 3 weeks (N = 8/group; values are means ± SEM).* P<0.05; ** P < 0.01 by two-sided student's t-test.**E.** Western blot analysis of Abca1 levels in primary mouse macrophages of WT and *MeXis*$^{-/-}$ mice treated with GW (0.5 μM for 16 hours). Actin was used as a loading control. The experiment repeated twice with similar results. **F.** Cholesterol efflux in the presence of ApoA-I or HDL from WT or *MeXis*$^{-/-}$ macrophages loaded with [^{3}H]cholesterol (1.0 μCi/ml) and treated with the acyl-CoA:cholesterol O-acyltransferase inhibitor (2 μg/ml) and either with DMSO or LXR ligand (1 μM GW3965). Experiments were conducted in triplicate. Data are expressed as mean ± SD. * P<0.05 by two-sided student's t-test.**G.** Cholesterol content measured in peritoneal macrophages isolated from mice on western diet for 12 weeks (N = 3/group). ** P < 0.01 by two-sided student's t-test**. H.** Oil-red-O staining of peritoneal macrophages isolated from WT or *MeXis*$^{-/-}$ mice and treated with oxidized LDL (100 μg/ml) for 72 h.The experiment was repeated 3 times with similar results.Scale bars, 50 μm. **I.** Total serum cholesterol levels in 10-week-old chow-fed male C57BL/6 mice transduced with adenoviral vectors encoding GFP control (Ad-GFP) or MeXis (Ad-MeXis) for 6 days (n = 8 per group). ** P < 0.01 by two-sided student's t-test. **J.** GFP and MeXis expression in liver 6 days after transduction of mice with Ad-GFP or Ad-MeXis, respectively (n = 8 per group except Abcg1 n=7 per group).* P<0.05; *** P < 0.001 by two-sided student's t-test. Data are expressed as mean ± SEM. **K.** Left, western blot analysis of Abca1 levels in liver from the mice in I (n = 4 per group). Right, quantification of protein levels normalized to actin. Data expressed as mean ± SD. *** P < 0.001 by two-sided student's t-test.

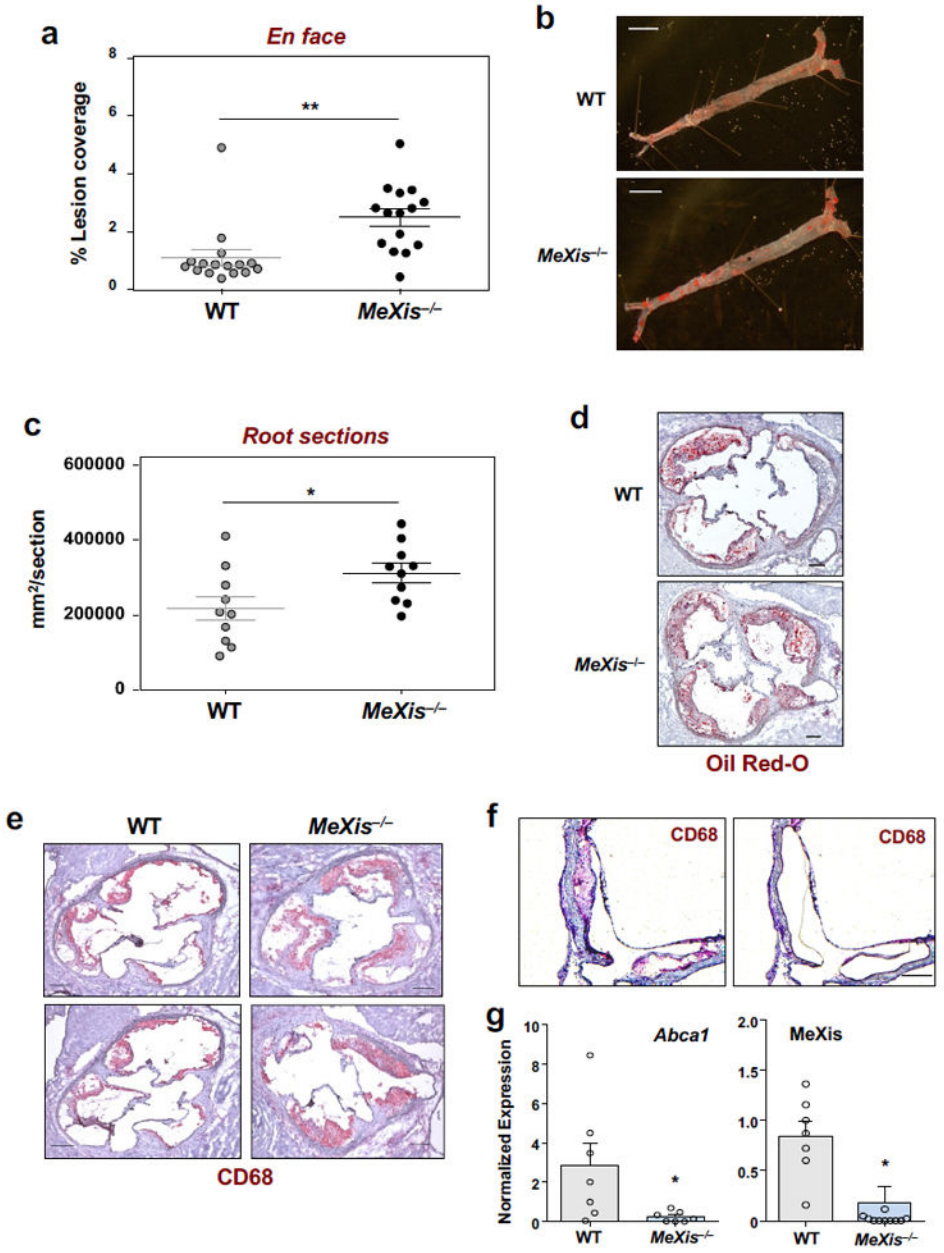

Figure 3. Loss of MeXis impairs macrophage *Abca1* expression and accelerates atherosclerosis

Ldlr$^{-/-}$ mice were transplanted with WT or *MeXis*$^{-/-}$ bone marrow and maintained on a Western diet for 17 weeks. **A.** Percentage of aorta surface area with atherosclerotic plaque by *en face* analysis. Data are mean ± SEM. (N = 16 WT, 15 MeXis). ** P < 0.01 by two-sided student's t-test**. B.** Representative photographs (from 16 WT and 15 *MeXis*$^{-/-}$) from *en face* analysis of aortas. Scale bars, 5 mm. **C.** Quantification of lesion area from oil-red O-stained aortic root sections. Mean ± SEM. (N = 10/ group). * P<0.05 by two-sided student's t-test. **D.** Oil Red-O staining of frozen sections from the aortic roots. Representative of 10 per group. Scale bars, 200 μm. **E.** Representative histology of the aortic root stained with the macrophage marker CD68 and H & E. Representative of 8 per group. Scale bars, 200 μm.**F.**

Representative images of an aortic lesion before and after laser capture microdissection of CD68-positive cells from *MeXis*$^{-/-}$ mice. Scale bar, 200 μm. **G.** *Abca1* and MeXis expression in laser capture samples as determined by realtime PCR. Samples taken from 6 animals WT and 4 *MeXis*$^{-/-}$. Number of samples for Abca1expression 7 per group and MeXis expression 7WT & 11*MeXis*$^{-/-}$. Data are mean ± SEM. * $P<0.05$ by two-sided student's t-test.

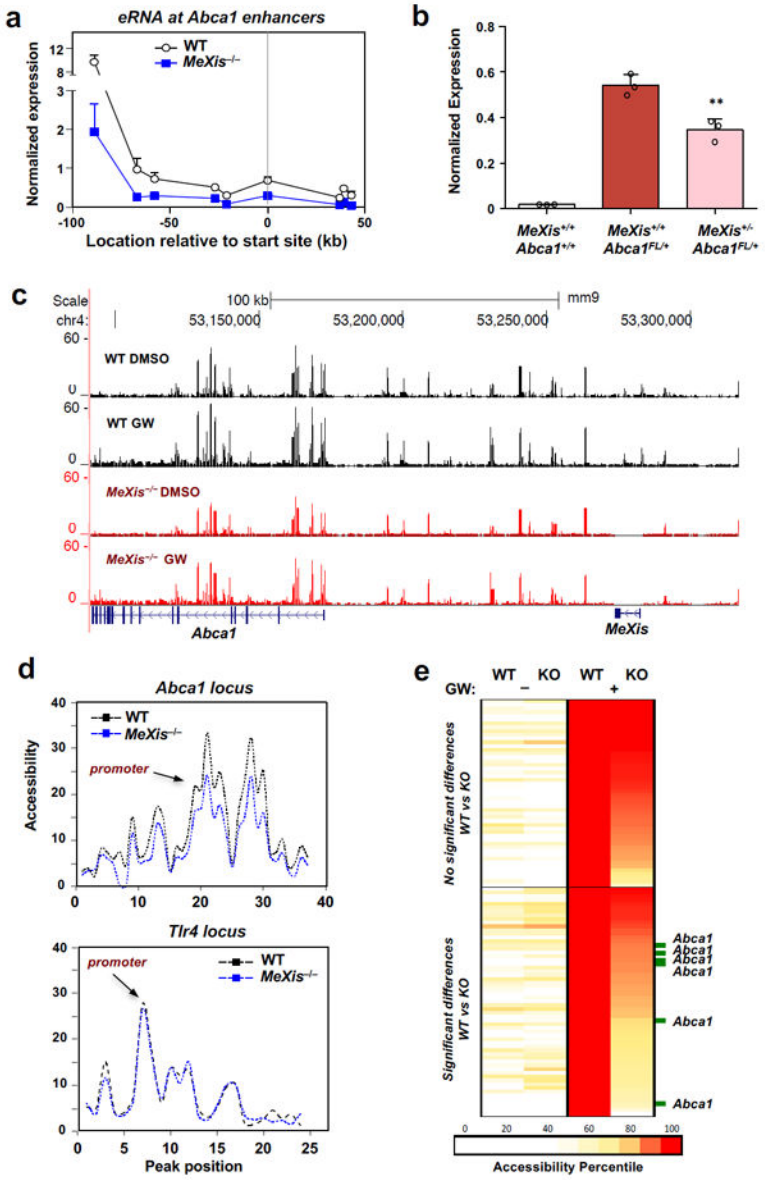

Figure 4. MeXis alters chromosome architecture at the *Abca1* locus

A. Gene expression of enhancer RNAs (short noncoding RNAs transcribed from enhancer elements)at the *Abca1* locus in primary mouse macrophages of WT or *MeXis*$^{-/-}$ mice treated with GW3965 (1 μM). The *x*-axis indicates the location at which gene expression was measured relative to the Abca1 transcription start site. N= 2WT, 3 *MeXis*$^{-/-}$. Mean ± SD. **B.** Expression from the *Abca1*^{FL} allele in primary macrophages from mice of the indicated genotypes (n=3/group). Mean ± SD.** P < 0.01 by two-sided student's t-test**. C.** Genome browser view of ATAC-seq data from primary mouse macrophages of WT or *MeXis*$^{-/-}$ mice treated with DMSO control or GW3965 (1 μM) for 3 h. Reads were from 4 individual samples per group. **D.** ATAC seq analysis showing accessibility at peaks around the *Abca1* and *Tlr4* genepromoters in WT or *MeXis*$^{-/-}$ macrophages with GW stimulation. Peak position arbitrary numbers the accessibility peaks shown in C at the Abca1 locus in

relationship to promoter TSS. **E.** Heat map of accessibility regions in WT and *MeXis*$^{-/-}$ macrophages with or without GW3965 treatment.Top of panel shows genome-wide accessibility sites significantly induced by GW3965 in both WT &*MeXis*$^{-/-}$ macrophages. Bottom panel shows accessibility sites significantly induced by GW3965 only WT macrophages.

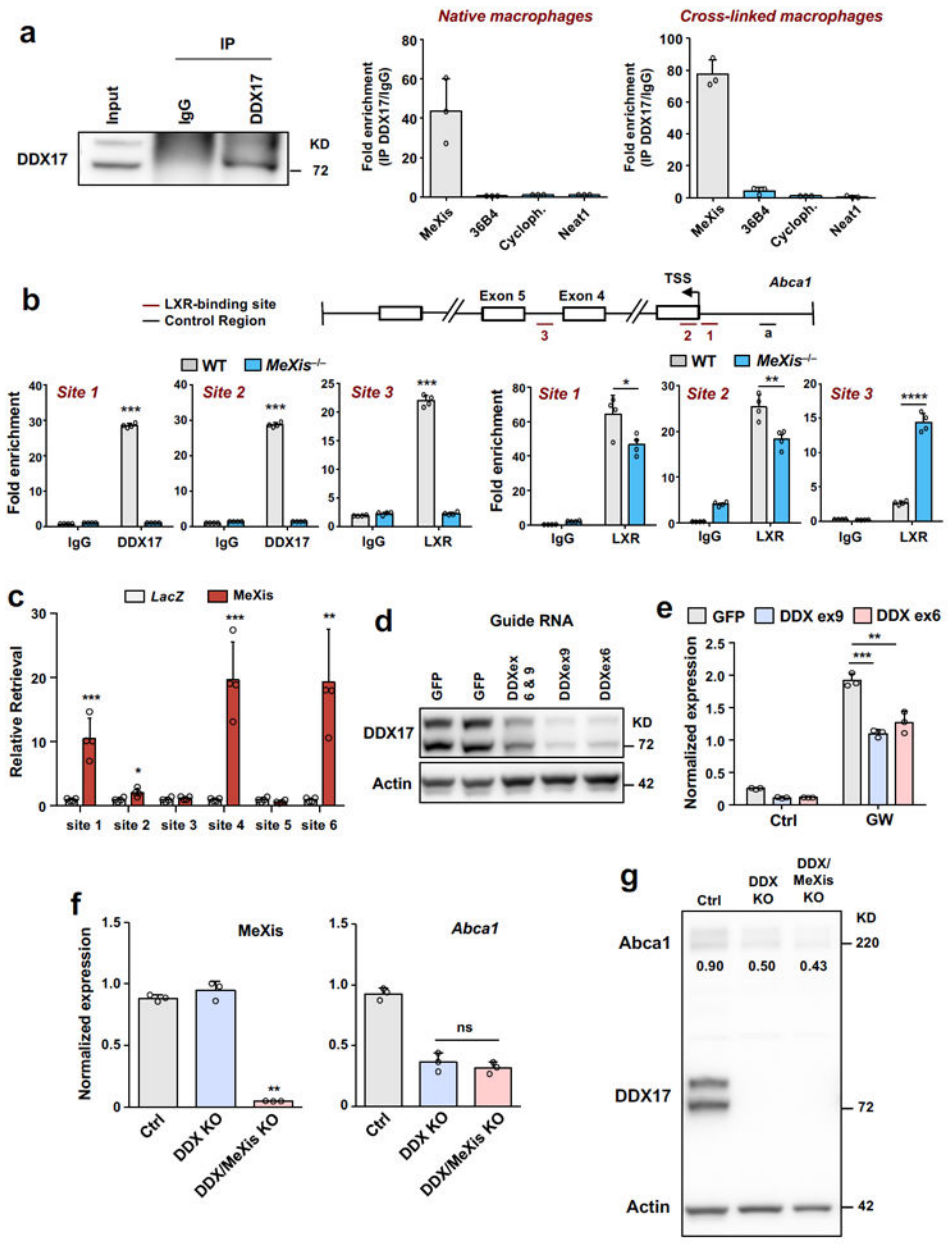

Figure 5. Identification of DDX17 as a binding partner of MeXis

A. RNA immunoprecipitation analysis of DDX17. Following immunoprecipitation using IgG control or DDX17 antibody from mouse peritoneal macrophages that were untreated or treated with the cross-linking agent formaldehyde,expression of MeXis, 36B4, cyclophilin (cyloph) and Neat1 was determined by qPCR analysis. N=3/group. Data are mean ± SD. **B.** Recruitment of DDX17 and LXR at the *Abca1* gene locus in mouse macrophages from WT or *MeXis*$^{-/-}$ mice as determined by ChIP qPCR analysis. Site 1, 2, and 3 are regions containing LXR binding elements known to bound LXR from Chip studies. Data are expressed as percent input retrieved normalized to an upstream control site (region a). N=4/ group. Data are mean ± SD. * P<0.05; ** P < 0.01; **** P < 0.0001 by two-sided student's

t-test. **C**. ChIRP-qPCR analysis of a series of ATAC-seq sites at the *Abca1* locus. Sites 1-6 are accessibility sites shown in figure 4e induced with LXR activation in WT but not *MeXis* $^{-/-}$ macrophages (n=4/group). Chirp probes designed against *LacZ* or MeXis. Mean ± SD. * P<0.05; ** P < 0.01; *** P < 0.001 by two-sided student's t-test. **D.** Western blot analysis of DDX17 levels in lentivirus-transduced immortalized iBMDM (pool of selection-positive cells). Lentiviruses contained either a GFP control or the indicated guide RNAs targeting the *DDX17* locus. Actin was used as a loading control.Representative of two independent western blots. **E.** *Abca1* expression in iBMDMs transduced with the indicated lentiviruses and treated with DMSO (Ctrl) or GW3965 (1 μM) for 12 hours (n= 3 per group). Data are mean ± SD. ** P < 0.01; *** P < 0.001 by Two-way ANOVA followed by two-sided student's t-test. **F.** *MeXis* or *Abca1* expression in iBMDMs (n= 3 per group). Ctrl is GFP, DDX is DDX17KO, DDXMeXKO is DDX17/*MeXis* double knockout. Data are mean ± SD. NS= Not significant at P < 0.05 by two-sided student's t-test. **G.** Western blot analysis of Abca1 and DDX17 levels in iBMDMs from F.Numbers in blot are quantitative Abca1 protein normalized to control (actin).

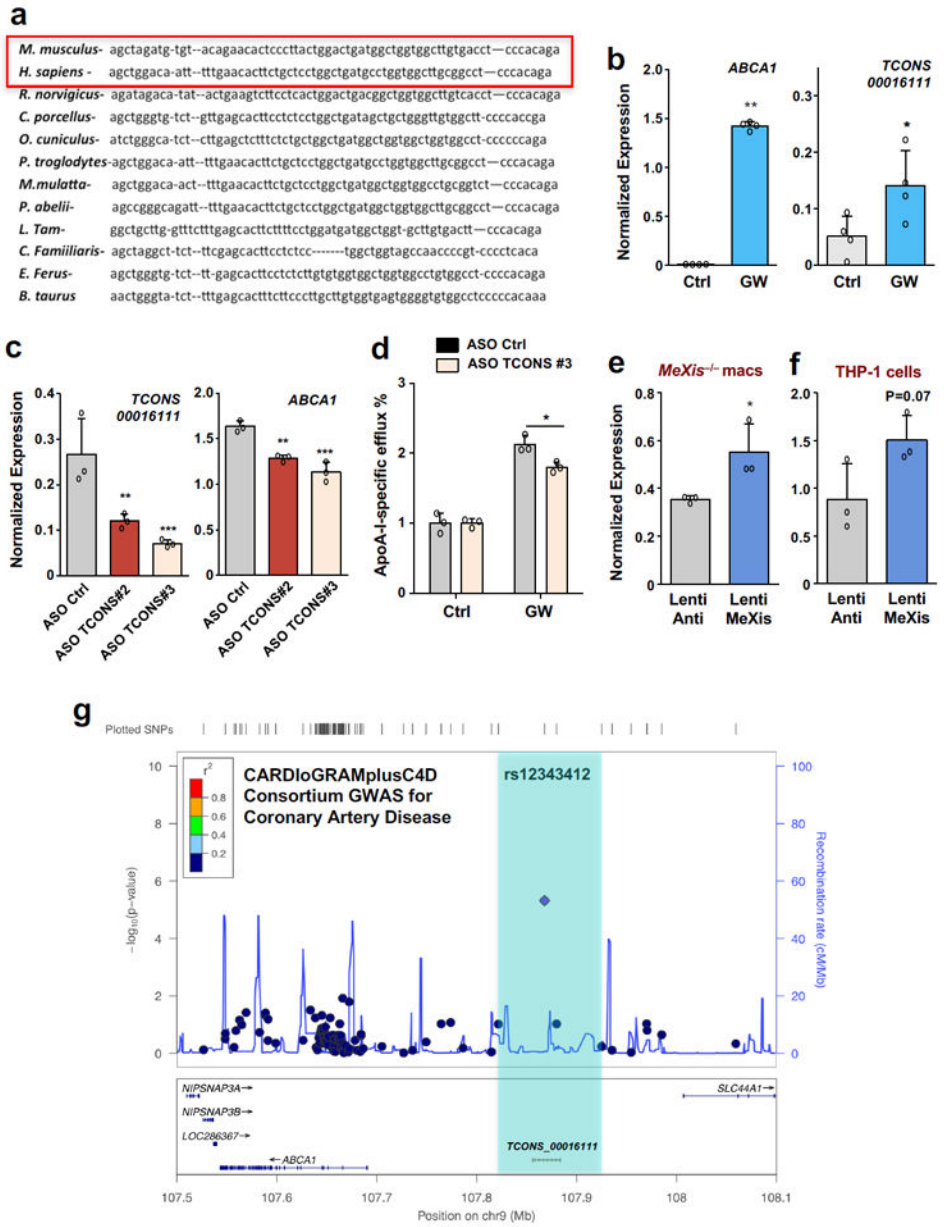

Figure 6. Functional conservation of the LXR-MeXis axis in humans

A. Sequence similarity across species at the *MeXis* gene locus. **B.** *ABCA1* and *TCONS00016111* expression in differentiated THP-1 monocytes treated with DMSO (Ctrl) or GW3965 (0.5 μM) for 16 hours (N=4 per group). Mean ± SD. * P < 0.05 by two-sided student's t-test. **C.** *ABCA1* and *TCONS00016111* expression in differentiated THP-1 cells treated with the indicated ASOs (50 nM) and GW3965 (0.5 μM) (N=3 per group). Data are mean ± SD. * P < 0.05; ** P < 0.01; *** P < 0.001 by one-way ANOVA followed by multiple comparisons test (Dunnett's).**D.** Cholesterol efflux in the presence of ApoA-I of THP-1 cells treated with the indicated ASO, loaded with [^{3}H]cholesterol (1.0 μCi/ml), and treated with acyl-CoA:cholesterol O-acyltransferase inhibitor (2 μg/ml) and with either DMSO or LXR ligand (1 μM GW3965) (n=3/group). Data are mean ± SD. * P < 0.05 by

two-sided student's t-test. **E.** *Abca1* gene expression in *MeXis*$^{-/-}$ BMDM macrophages treated with control (antisense MeXis) or MeXis lentivirus (n=3 per group). Data are mean ± SD. * $P < 0.05$ by two-sided student's t-test. **F.** *Abca1* expression in THP-1 cells treated with control or MeXis lentivirus (n=3 per group).Mean ± Two-sided student's t-test. Not significant at $P<0.05$. 95% Confidence Interval (-0.1025 to 1.338). **G.** Regional association plot of variants at *TCONS-0016111* and the risk of coronary artery disease in humans from the CARDIoGRAMplusC4D Consortium.